

1 Functional MRI brain state 2 occupancy in the presence of 3 cerebral small vessel disease – 4 pre-registration for a multiverse 5 replication analysis of the Hamburg 6 City Health Study

✉ For correspondence:
e.schlemm@uke.de

Present address:
Dr. Dr. Eckhard Schlemm,
Klinik und Poliklinik für
Neurologie,
Universitätsklinikum
Hamburg-Eppendorf,
Martinistr. 52,
D-20251 Hamburg

Data availability:
Preprocessed data will be
available e.g. on
<https://github.com/csi-hamburg/HCHS-brain-states-RR>.

Funding: Deutsche
Forschungsgemeinschaft
(DFG) - 178316478 - C2

Competing interests: The
author declares no
competing interests.

7 Eckhard Schlemm, MBBS PhD  

8 1Department of Neurology, University Medical Center
9 Hamburg-Eppendorf

11 Abstract

12 **Objective:** To replicate recent findings about the association between the extent of
13 cerebral small vessel disease (cSVD), functional brain network dedifferentiation and
14 cognitive impairment.
15 **Methods:** We will analyze demographic, imaging and behavioral data from the
16 prospective population-based Hamburg City Health Study. Using a fully prespecified
17 analysis pipeline, we will estimate discrete brain states from structural and resting-state
18 functional magnetic resonance imaging (MRI). In a multiverse analysis we will vary brain
19 parcellations and functional MRI confound regression strategies. Severity of cSVD will
20 be operationalised as the volume of white matter hyperintensities of presumed
21 vascular origin. Processing speed and executive dysfunction are quantified by the trail
22 making test (TMT).
23 **Hypotheses:** We hypothesize a) that greater volume of supratentorial white matter

²⁴ hyperintensities is associated with less time spent in functional MRI-derived brain
²⁵ states of high fractional occupancy; and b) that less time spent in these high-occupancy
²⁶ brain states is associated with longer time to completion in part B of the TMT.

²⁷

²⁸ Introduction

²⁹ Cerebral small vessel disease (cSVD) is an arteriolopathy of the brain, associated with
³⁰ age and common cardiovascular risk factors (Wardlaw, C. Smith, and Dichgans, 2013).
³¹ cSVD predisposes to ischemic, in particular lacunar, stroke and may lead to cognitive im-
³² pairment and dementia (Cannistraro et al., 2019). Neuroimaging findings in cSVD reflect
³³ its underlying pathology (Wardlaw, Valdés Hernández, and Muñoz-Maniega, 2015) and
³⁴ include white matter hyperintensities (WMH) and lacunes of presumed vascular origin,
³⁵ small subcortical infarcts and microbleeds, enlarged perivascular spaces as well as brain
³⁶ atrophy (Wardlaw, E. E. Smith, et al., 2013). However, the extent of visible cSVD features
³⁷ on magnetic resonance imaging (MRI) is an imperfect predictor of the severity of clini-
³⁸ cal sequelae (Das et al., 2019), and our understanding of the causal mechanisms linking
³⁹ cSVD-associated brain damage to clinical deficits remains limited (Bos et al., 2018).

⁴⁰ Recent efforts have concentrated on exploiting network aspects of the structural (Tu-
⁴¹ ladhar, Dijk, et al., 2016; Tuladhar, Tay, et al., 2020; Lawrence, Zeestraten, et al., 2018) and
⁴² functional (Dey et al., 2016; Schulz et al., 2021) organization of the brain to understand
⁴³ the relation between cSVD and clinical deficits in cognition and other domains reliant
⁴⁴ on distributed processing. Reduced structural network efficiency has repeatedly been
⁴⁵ described as a causal factor in the development of cognitive impairment, in particular
⁴⁶ executive dysfunction, in cSVD (Lawrence, Chung, et al., 2014; Shen et al., 2020; Reijmer
⁴⁷ et al., 2016; Prins et al., 2005). Findings with respect to functional connectivity results, on
⁴⁸ the other hand, are more heterogeneous, perhaps due to its limited reproducibility in
⁴⁹ the presence of cSVD and dependence on arbitrary processing choices (Lawrence, Tozer,
⁵⁰ et al., 2018; Gesierich et al., 2020). As a promising new avenue, time-varying, or dynamic,
⁵¹ functional connectivity approaches have more recently been explored in patients with
⁵² subcortical ischemic vascular disease (Yin et al., 2022; Xu et al., 2021).

⁵³ In the present paper, we aim to replicate and extend the main results of (Schlemm
⁵⁴ et al., 2022); in this recent study, the authors analyzed MR imaging and clinical data from
⁵⁵ the prospective Hamburg City Health Study (HCHS, (Jagodzinski et al., 2020)) using a coac-

Question	Hypothesis	Sampling plan	Analysis plan	Rationale deciding sensitivity for the test	Interpretation given different outcomes	Theory that could be shown wrong by the outcome
Is severity of cerebral small vessel disease, quantified by the volume supratentorial white matter hyperintensities of presumed vascular origin (WMH), associated with time spent in high-occupancy brain states, defined by resting-state functional MRI	Higher WMH volume is associated with lower average occupancy of the two highest-occupancy brain states	Available subjects with clinical and imaging data from the HCHS (Jagodzinski et al., 2020)	Standardized preprocessing of structural and functional MRI data • automatic quantification of WMH • co-activation pattern analysis • multivariable generalised regression analyses	Tradition	$P < 0.05 \rightarrow$ rejection of the null hypothesis of no association between cSVD and fractional occupancy; $P > 0.05 \rightarrow$ insufficient evidence to reject the null hypothesis	Functional brain dynamics are not related to subcortical ischemic vascular disease.

Table 1. Study Design Template

⁵⁶ tivation pattern approach to define discrete brain states and found associations between
⁵⁷ the WMH load, time spent in high-occupancy brain states characterized by activation or
⁵⁸ suppression of the default mode network (DMN) and executive dysfunction.
⁵⁹ Our primary hypothesis is that the volume of supratentorial white matter hyperinten-
⁶⁰ sities is associated with the fractional occupancy (defined below) of DMN-related brain
⁶¹ states in a middle-aged to elderly population mildly affected by cSVD. Our second hypoth-
⁶² esis is that this fractional occupancy is associated with executive dysfunction, measured
⁶³ as the time to complete part B of the trail making test (TMT).
⁶⁴ Both hypotheses will be tested in an independent subsample of the HCHS study popu-
⁶⁵ lation using the same imaging protocols, examination procedures and analysis pipelines
⁶⁶ as in (Schlemm et al., 2022). The robustness of associations will be explored in a multi-
⁶⁷ verse approach by varying key steps in the analysis pipeline.

⁶⁸ Methods

⁶⁹ Study population

⁷⁰ The paper will analyze data from the Hamburg City Health Study (HCHS), which is an
⁷¹ ongoing prospective, population-based cohort study aiming to recruit a cross-sectional
⁷² sample of 45 000 adult participants from the city of Hamburg, Germany (Jagodzinski et
⁷³ al., 2020). From the first 10 000 participants of the HCHS we will aim to include those
⁷⁴ who were documented to have received brain imaging ($n=2652$) and exclude those who
⁷⁵ were analyzed in our previous report (Schlemm et al., 2022). The ethical review board of
⁷⁶ the Landesärztekammer Hamburg (State of Hamburg Chamber of Medical Practitioners)
⁷⁷ approved the HCHS (PV5131), all participants provided written informed consent.

78 Demographic and clinical characterization

79 From the study database we will extract participants' age at the time of inclusion in years,
80 their self-reported gender and the number of years spent in education. During the visit
81 at the study center, participants undergo cognitive assessment using standardized tests.
82 We will extract from the database their performance scores in the Trail Making Test part B,
83 measured in seconds, as an operationalization of executive function (Tombaugh, 2004).

84 MRI acquisition and preprocessing

85 The magnetic resonance imaging protocol for the HCHS includes structural and resting-
86 state functional sequences. The acquisition parameters on a 3 T Siemens Skyra MRI scan-
87 ner (Siemens, Erlangen, Germany) have been reported before (Petersen et al., 2020; Frey
88 et al., 2021) and are given as follows:

89 For T_1 -weighted anatomical images, a 3D rapid acquisition gradient-echo sequence
90 (MPRAGE) was used with the following sequence parameters: repetition time TR = 2500 ms,
91 echo time TE = 2.12 ms, 256 axial slices, slice thickness ST = 0.94 mm, and in-plane resolu-
92 tion IPR = $(0.83 \times 0.83) \text{ mm}^2$.

93 T_2 -weighted fluid attenuated inversion recovery (FLAIR) images were acquired with
94 the following sequence parameters: TR = 4700 ms, TE = 392 ms, 192 axial slices, ST =
95 0.9 mm, IPR = $(0.75 \times 0.75) \text{ mm}^2$.

96 125 resting state functional MRI volumes were acquired (TR = 2500 ms; TE = 25 ms;
97 flip angle = 90°; slices = 49; ST = 3 mm; slice gap = 0 mm; IPR = $(2.66 \times 2.66) \text{ mm}^2$). Subjects
98 were asked to keep their eyes open and to think of nothing.

99 We will verify the presence and voxel-dimensions of expected MRI data for each par-
100 ticipant and exclude those for whom at least one of T_1 -weighted, FLAIR and resting-state
101 MRI is missing. To ensure reproducibility, no visual quality assessment on raw images
102 will be performed.

103 For the remaining participants, structural and resting-state functional MRI data will
104 be preprocessed using FreeSurfer v6.0 (<https://surfer.nmr.mgh.harvard.edu/>), and fmriPrep
105 v20.2.6 (Esteban et al., 2019), using default parameters. Participants will be excluded if
106 automated processing using at least one of these packages fails.

107 Quantification of WMH load

108 For our primary analysis, the extent of ischemic white matter disease will be operational-
109 ized as the total volume of supratentorial WMHs obtained from automated segmentation
110 using a combination of anatomical priors, BIANCA (Griffanti, Zamboni, et al., 2016) and
111 LOCATE (Sundaresan et al., 2019), post-processed with a minimum cluster size of 30 vox-
112 els, as described in (Schlemm et al., 2022). In an exploratory analysis, we partition voxels
113 identified as WMH into deep and periventricular components according to their distance
114 to the ventricular system (cut-off 10 mm, (Griffanti, Jenkinson, et al., 2018))

115 Brain state estimation

116 Output from fMRIprep will be post-processed using xcpEngine v1.2.1 to obtain de-confounded
117 spatially averaged BOLD time series (Ciric, Wolf, et al., 2017). For the primary analysis we
118 will use the *36p* regression strategy and the Schaefer-400 parcellation (Schaefer et al.,
119 2018), as in (Schlemm et al., 2022).

120 Different atlases and confound regression strategies, as implemented in xcpEngine,
121 will be included in the exploratory multiverse analysis.

122 Co-activation pattern (CAP) analysis will be performed by first aggregating parcellated,
123 de-confounded BOLD signals into a ($n_{\text{parcels}} \times \sum_i n_{\text{time points},i}$) feature matrix, where $n_{\text{time points},i}$
124 denotes the number of retained volumes for subject i after confound regression. Cluster-
125 ing will be performed using the k -means algorithm ($k = 5$) with distance measure given
126 by 1 minus the sample Pearson correlation between points, as implemented in Matlab
127 R2021a. We will estimate subject- and state-specific fractional occupancies, which are
128 defined as the proportion of BOLD volumes assigned to each brain state (Vidaurre et al.,
129 2018). The two states with the highest average occupancy will be identified as the basis
130 for further analysis.

131 Statistical analysis

132 For demographic (age, gender, years of education) and clinical (TMT-B) variables the num-
133 ber of missing records will be reported. For non-missing values, we will provide descrip-
134 tive summary statistics using median and interquartile range. The proportion of men
135 and women in the sample will be reported.

136 As a first outcome-neutral quality check of the implementation of the MRI process-
137 ing pipeline, brain state estimation and co-activation pattern analysis, we will compare

¹³⁸ fractional occupancies between brain states. We expect that the average fractional oc-
¹³⁹ cupancy in two high-occupancy states is higher than the average fractional occupancy in
¹⁴⁰ the other three states. Point estimates and 95% confidence intervals will be presented
¹⁴¹ for the difference in average fractional occupancy to check this assertion.

¹⁴² For further analyses, non-zero WMH volumes will be subjected to a logarithmic trans-
¹⁴³ formation. Zero values will retain their value zero; to compensate, all models will include
¹⁴⁴ a binary indicator for zero WMH volume if at least one non-zero value is present.

¹⁴⁵ To assess the primary hypothesis of a negative association between the extent of is-
¹⁴⁶ chemic white matter disease and time spent in high-occupancy brain states, we will per-
¹⁴⁷ form a fixed-dispersion beta-regression to model the logit of the conditional expectation
¹⁴⁸ of the average fractional occupancy of two high-occupancy states as an affine function of
¹⁴⁹ the logarithmized WMH load. Age and gender will be included as covariates. The strength
¹⁵⁰ of the association will be quantified as an odds ratio per interquartile ratio of the WMH
¹⁵¹ burden distribution and accompanied by a 95% confidence interval. Significance testing
¹⁵² of the null hypothesis of no association will be conducted at the conventional significance
¹⁵³ level of 0.05. Estimation and testing will be carried out using the 'betareg' package v3.1.4
¹⁵⁴ in R v4.2.1.

¹⁵⁵ To assess the secondary hypothesis of an association between time spent in high-
¹⁵⁶ occupancy brain states and executive dysfunction, we will perform a generalized linear
¹⁵⁷ regression with a Gamma response distribution to model the logarithm of the condi-
¹⁵⁸ tional expected completion time in part B of the TMT as an affine function of the average
¹⁵⁹ fractional occupancy of two high-occupancy states. Age, gender, years of education and
¹⁶⁰ logarithmized WMH load will be included as covariates. The strength of the association
¹⁶¹ will be quantified as a multiplicative factor per percentage point and accompanied by a
¹⁶² 95% confidence interval. Significance testing of the null hypothesis of no association will
¹⁶³ be conducted at the conventional significance level of 0.05. Estimation and testing will
¹⁶⁴ be carried out using the glm function included in the 'stats' package from R v4.2.1.

¹⁶⁵ Sample size calculation is based on the data presented in (Schlemm et al., 2022),
¹⁶⁶ where an odds ratio of 0.95 was reported as the primary effect size of interest. We used
¹⁶⁷ simple bootstrapping to create 10 000 hypothetical datasets of size 200, 400, 600, 800, 900,
¹⁶⁸ 910, ..., 1100, 1200, 1400, 1500, 1600. Each dataset was subjected to the estimation pro-
¹⁶⁹ cedure described above. For each sample size, the proportion of datasets in which the
¹⁷⁰ primary null hypothesis of no association between fractional occupancy and WMH load

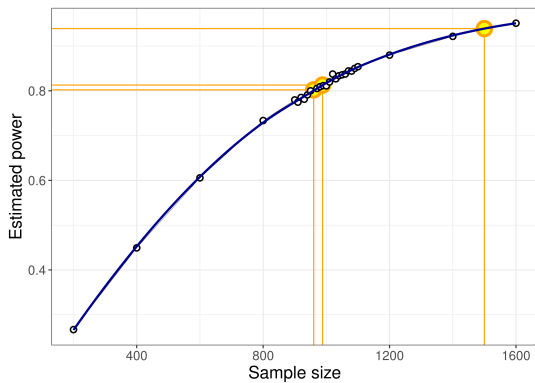


Figure 1. Estimated power for different sample sizes is obtained as the proportion of synthetic data sets in which the null hypothesis of no association between WMH volume and time spent in high-occupancy brain states can be rejected at the $\alpha = 0.05$ significance level. Proportions are based on a total of 10 000 synthetic data sets obtained by bootstrapping the data presented in (Schlemm et al., 2022). Highlighted in orange are the smallest sample size ensuring a power of at least 80 % ($n = 960$), the sample size of the pilot data ($n = 988$, post-hoc power 81.3 %), and the expected sample sample size for this replication study ($n = 1500$, a-priori power 93.9 %).

¹⁷¹ could be rejected at $\alpha = 0.05$ was computed and is recorded as a power curve in Figure 1.
¹⁷² It is seen that a sample size of 960 would allow replication of the reported effect with
¹⁷³ a power of 80.2 %. We anticipate a sample size of 1500, which yields a power of 93.9 %.

¹⁷⁴ Multiverse analysis

¹⁷⁵ Both in (Schlemm et al., 2022) and for our primary replication analysis we made cer-
¹⁷⁶ tain analytical choices in the operationalisation of brain states and ischemic white mat-
¹⁷⁷ ter disease, namely the use of the $36p$ confound regression strategy, the Schaefer-400
¹⁷⁸ parcellation and a BIANCA/LOCATE-based WMH segmentation algorithm. If the hypoth-
¹⁷⁹ esized association between WMH burden and time spent in high-occupancy states can
¹⁸⁰ be replicated using these primary analytical choices, its robustness with regard to other
¹⁸¹ choices will be explored in a multiverse analysis (Schlemm et al., 2022; Steegen et al.,
¹⁸² 2016). Specifically, we will estimate brain states from BOLD time series processed ac-
¹⁸³ cording to a variety of established confound regression strategies and aggregated over
¹⁸⁴ different cortical brain parcellations (Table 2, Ceric, Rosen, et al., 2018; Ceric, Wolf, et al.,
¹⁸⁵ 2017). Extent of cSVD will additionally be quantified by the volume of deep and periven-
¹⁸⁶ tricular white matter hyperintensities.

¹⁸⁷ For each combination of analytical choice of confound regression strategy, parcella-
¹⁸⁸ tion and subdivision of white matter lesion load ($9 \times 9 \times 3 = 243$ scenarios in total) we will
¹⁸⁹ quantify the association between WMH load and average time spent in high-occupancy
¹⁹⁰ brain states using odds ratio and 95 % confidence intervals as described above. No hy-

Name of the atlas	#parcels	Reference	Design	Reference
Desikan-Killiany	86	Desikan et al., 2006	24p	Friston et al., 1996
AAL	116	Tzourio-Mazoyer et al., 2002	24p + GSR	Macey et al., 2004
Harvard-Oxford	112	Makris et al., 2006	36p	Satterthwaite et al., 2013
glasser360	360	Glasser et al., 2016	26p + spike regression	Cox, 1996
gordon333	333	Gordon et al., 2016	36p + despiking	Satterthwaite et al., 2013
power264	264	Power, Cohen, et al., 2011	36p + scrubbing	Power, Mitra, et al., 2014
schaefer{N}	100	Schaefer et al., 2018	aCompCor	Muschelli et al., 2014
	200		tCompCor	Behzadi et al., 2007
	400		AROMA	Pruim et al., 2015

AAL: Automatic Anatomical Labelling

(a) Parcellations

GSR: Global signal regression, AROMA: bla

(b) Confound regression strategies, adapted from (Ciric, Wolf, et al., 2017)

Table 2. Multiverse analysis, implemented using xcpEngine (Ciric, Rosen, et al., 2018)

191 hypothesis testing and, therefore, no adjustment for multiple testing, will be carried out in
 192 these non-primary analyses.

193 Exploratory analysis

194 In previous work, two high-occupancy brain states were related to the default-mode net-
 195 work (Cornblath et al., 2020). We will further explore this relation by computing, for each
 196 individual brain state, the cosine similarity of the positive and negative activations of
 197 the cluster's centroid with a set of a-priori defined functional 'communities' or networks
 198 (Schaefer et al., 2018; Yeo et al., 2011). Results will be thus visualized as spider plots for
 199 the Schaefer, Gordon and Power atlases.

200 Code and pilot data

201 Summary data from the first 1000 imaging data points of the HCHS have been published
 202 with (Schlemm et al., 2022) and form the basis for the hypotheses tested in this replication
 203 study. We have implemented our prespecified analysis pipeline described above in R
 204 and Matlab, and applied it to this previous sample. Data, code and results have been
 205 stored on GitHub (https://github.com/csi-hamburg/HCHS_brain_states_RR) und preserved
 206 on Zenodo.

207 Thus re-analysing data from 988 subjects, the separation between two high-occupancy
 208 and three low-occupancy brain states could be reproduced for all combinations of brain
 209 parcellation and confound regression strategies (Figure 2).

210 In a multiverse analysis, the main finding was somewhat robust with respect to these
 211 choices: a statistically significant negative association between WMH load and time spent
 212 in high-occupancy states was observed in 18/81 scenarios, with 5/81 statistically signifi-

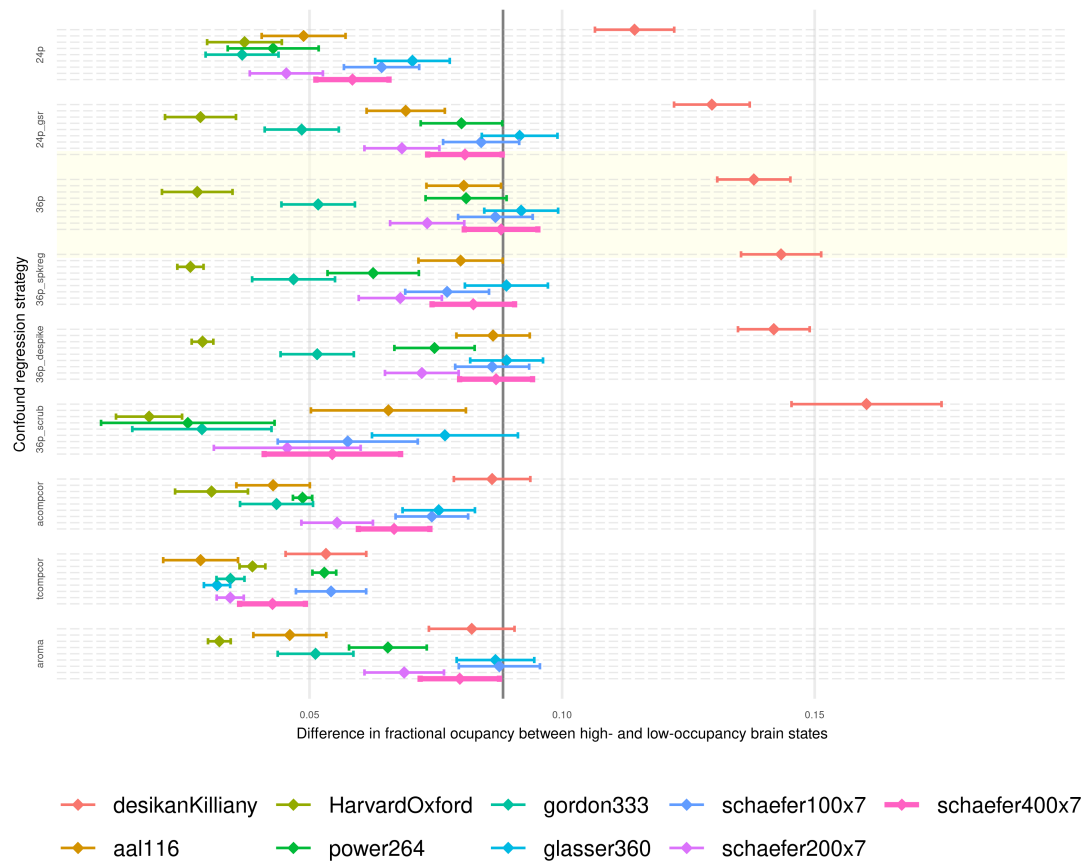


Figure 2. Point estimates and 95 % confidence intervals for the mean in fractional occupancy between high- and low occupancy states are shown for different confound regression strategies and brain parcellations. The primary choices (36p and schaefer400) are highlighted by a yellow box and thick pink line, respectively. The effect size reported in (Schlemm et al., 2022) is indicated by a vertical line at 0.08830623.

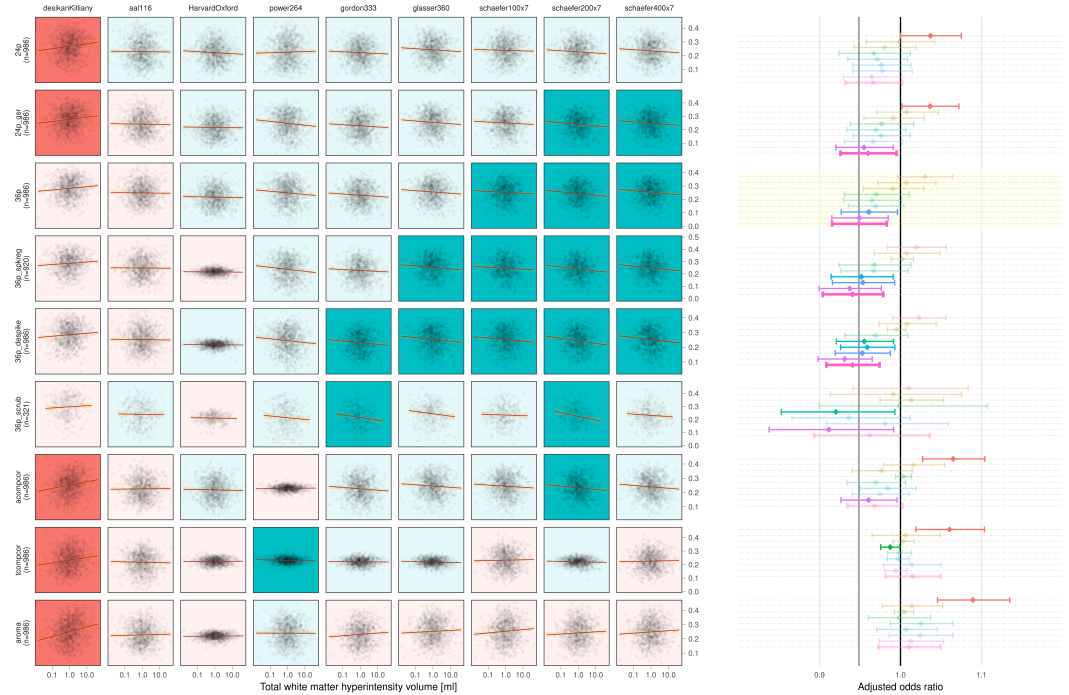


Figure 3. On the left, scatter plots of average fractional occupancies in high-occupancy states against WMH volume on a logarithmic scale (base 10 for easier visualization) for different combinations of confound regression strategies and brain parcellations. Linear regression lines indicate the direction of the unadjusted association between $\log(\text{WMH})$ and occupancy. Background color of individual panels indicates the direction of the association after adjustment for age, sex and zero WMH volume (green, negative; red, positive). A pale background indicates that the association between $\log(\text{WMH})$ and average occupancy is not statistically different from zero. On the right, the same information is shown using point estimates and 95 % confidence intervals for the adjusted odds ratio of the association.

213 can positive associations occurring with the Desikan–Killiany parcellation only (Figure 3).
 214 The secondary finding of an association between greater TMT-B times and lower frac-
 215 tional occupancy was similarly robust with 12/81 statistically significant negative and no
 216 statistically significant positive associations.

217 Timeline and access to data

218 At the time of planning of this study, all demographic, clinical and imaging data used in
 219 this analysis have been collected by the HCHS and are held in the central trial database.
 220 Quality checks for non-imaging variables have been performed centrally. WMH segmen-
 221 tation based on structural MRI data of the first 10 000 participants of the HCHS has been
 222 performed previously using the BIANCA/LOCATE approach (Rimmele et al., 2022) and re-
 223 sults are included in this preregistration ([./derivatives/WMH/cSVD_all.csv](#)). Functional
 224 MRI data and clinical measures of executive dysfunction (TMT-B scores) have not been
 225 analyzed by the author. Analysis of the data will begin immediately after acceptance-in-

²²⁶ principle of the stage 1 submission of the registered report is obtained. Submission of
²²⁷ the full manuscript (stage 2) is planned two months later.

²²⁸ Acknowledgment

²²⁹ This preprint was created using the LaPreprint template ([https://github.com/roaldarbol/](https://github.com/roaldarbol/lapreprint)
²³⁰ [lapreprint](#)) by Mikkel Roald-Arbøl .

²³¹ References

- ²³² Behzadi, Yashar et al. (2007). "A component based noise correction method (CompCor)
²³³ for BOLD and perfusion based fMRI". In: *Neuroimage* 37.1, pp. 90–101.
- ²³⁴ Bos, Daniel et al. (2018). "Cerebral small vessel disease and the risk of dementia: A sys-
²³⁵ tematic review and meta-analysis of population-based evidence". en. In: *Alzheimers.*
²³⁶ *Dement.* 14.11, pp. 1482–1492.
- ²³⁷ Cannistraro, Rocco J et al. (2019). "CNS small vessel disease: A clinical review". en. In: *Neu-*
²³⁸ *rology* 92.24, pp. 1146–1156.
- ²³⁹ Ceric, Rastko, Adon FG Rosen, et al. (2018). "Mitigating head motion artifact in functional
²⁴⁰ connectivity MRI". In: *Nature protocols* 13.12, pp. 2801–2826.
- ²⁴¹ Ceric, Rastko, Daniel H Wolf, et al. (2017). "Benchmarking of participant-level confound
²⁴² regression strategies for the control of motion artifact in studies of functional con-
²⁴³ nectivity". en. In: *Neuroimage* 154, pp. 174–187.
- ²⁴⁴ Cornblath, Eli J et al. (2020). "Temporal sequences of brain activity at rest are constrained
²⁴⁵ by white matter structure and modulated by cognitive demands". en. In: *Commun Biol*
²⁴⁶ 3.1, p. 261.
- ²⁴⁷ Cox, Robert W (1996). "AFNI: software for analysis and visualization of functional mag-
²⁴⁸ netic resonance neuroimages". In: *Computers and Biomedical research* 29.3, pp. 162–
²⁴⁹ 173.
- ²⁵⁰ Das, Alvin S et al. (2019). "Asymptomatic Cerebral Small Vessel Disease: Insights from
²⁵¹ Population-Based Studies". en. In: *J. Stroke Cerebrovasc. Dis.* 21.2, pp. 121–138.
- ²⁵² Desikan, Rahul S et al. (2006). "An automated labeling system for subdividing the human
²⁵³ cerebral cortex on MRI scans into gyral based regions of interest". In: *Neuroimage* 31.3,
²⁵⁴ pp. 968–980.
- ²⁵⁵ Dey, Ayan K et al. (2016). "Pathoconnectomics of cognitive impairment in small vessel
²⁵⁶ disease: A systematic review". en. In: *Alzheimers. Dement.* 12.7, pp. 831–845.

- ²⁵⁷ Esteban, Oscar et al. (2019). "fMRIPrep: a robust preprocessing pipeline for functional
²⁵⁸ MRI". en. In: *Nat. Methods* 16.1, pp. 111–116.
- ²⁵⁹ Frey, Benedikt M et al. (2021). "White matter integrity and structural brain network topol-
²⁶⁰ ogy in cerebral small vessel disease: The Hamburg city health study". en. In: *Hum. Brain
261 Mapp.* 42.5, pp. 1406–1415.
- ²⁶² Friston, Karl J et al. (1996). "Movement-related effects in fMRI time-series". In: *Magnetic
263 resonance in medicine* 35.3, pp. 346–355.
- ²⁶⁴ Gesierich, Benno et al. (2020). "Alterations and test-retest reliability of functional connec-
²⁶⁵ tivity network measures in cerebral small vessel disease". en. In: *Hum. Brain Mapp.*
²⁶⁶ 41.10, pp. 2629–2641.
- ²⁶⁷ Glasser, Matthew F et al. (2016). "A multi-modal parcellation of human cerebral cortex".
²⁶⁸ en. In: *Nature* 536.7615, pp. 171–178.
- ²⁶⁹ Gordon, Evan M et al. (2016). "Generation and Evaluation of a Cortical Area Parcellation
²⁷⁰ from Resting-State Correlations". en. In: *Cereb. Cortex* 26.1, pp. 288–303.
- ²⁷¹ Griffanti, Ludovica, Mark Jenkinson, et al. (2018). "Classification and characterization of
²⁷² periventricular and deep white matter hyperintensities on MRI: A study in older adults".
²⁷³ en. In: *Neuroimage* 170, pp. 174–181.
- ²⁷⁴ Griffanti, Ludovica, Giovanna Zamboni, et al. (2016). "BIANCA (Brain Intensity AbNormal-
²⁷⁵ ity Classification Algorithm): A new tool for automated segmentation of white matter
²⁷⁶ hyperintensities". en. In: *Neuroimage* 141, pp. 191–205.
- ²⁷⁷ Jagodzinski, Annika et al. (2020). "Rationale and Design of the Hamburg City Health Study".
²⁷⁸ en. In: *Eur. J. Epidemiol.* 35.2, pp. 169–181.
- ²⁷⁹ Lawrence, Andrew J, Ai Wern Chung, et al. (2014). "Structural network efficiency is as-
²⁸⁰ sociated with cognitive impairment in small-vessel disease". en. In: *Neurology* 83.4,
²⁸¹ pp. 304–311.
- ²⁸² Lawrence, Andrew J, Daniel J Tozer, et al. (2018). "A comparison of functional and trac-
²⁸³ tography based networks in cerebral small vessel disease". en. In: *Neuroimage Clin* 18,
²⁸⁴ pp. 425–432.
- ²⁸⁵ Lawrence, Andrew J, Eva A Zeestraten, et al. (2018). "Longitudinal decline in structural
²⁸⁶ networks predicts dementia in cerebral small vessel disease". en. In: *Neurology* 90.21,
²⁸⁷ e1898–e1910.
- ²⁸⁸ Macey, Paul M et al. (2004). "A method for removal of global effects from fMRI time series".
²⁸⁹ In: *Neuroimage* 22.1, pp. 360–366.

- 290 Makris, Nikos et al. (2006). "Decreased volume of left and total anterior insular lobule in
291 schizophrenia". In: *Schizophrenia research* 83.2-3, pp. 155–171.
- 292 Muschelli, John et al. (2014). "Reduction of motion-related artifacts in resting state fMRI
293 using aCompCor". In: *Neuroimage* 96, pp. 22–35.
- 294 Petersen, Marvin et al. (2020). "Network Localisation of White Matter Damage in Cerebral
295 Small Vessel Disease". en. In: *Sci. Rep.* 10.1, p. 9210.
- 296 Power, Jonathan D, Alexander L Cohen, et al. (2011). "Functional network organization of
297 the human brain". en. In: *Neuron* 72.4, pp. 665–678.
- 298 Power, Jonathan D, Anish Mitra, et al. (2014). "Methods to detect, characterize, and re-
299 move motion artifact in resting state fMRI". In: *Neuroimage* 84, pp. 320–341.
- 300 Prins, Niels D et al. (2005). "Cerebral small-vessel disease and decline in information pro-
301 cessing speed, executive function and memory". en. In: *Brain* 128.Pt 9, pp. 2034–2041.
- 302 Pruim, Raimon HR et al. (2015). "ICA-AROMA: A robust ICA-based strategy for removing
303 motion artifacts from fMRI data". In: *Neuroimage* 112, pp. 267–277.
- 304 Reijmer, Yael D et al. (2016). "Small vessel disease and cognitive impairment: The rele-
305 vance of central network connections". en. In: *Hum. Brain Mapp.* 37.7, pp. 2446–2454.
- 306 Rimmeli, David Leander et al. (2022). "Association of Carotid Plaque and Flow Velocity
307 With White Matter Integrity in a Middle-aged to Elderly Population". en. In: *Neurology*.
- 308 Satterthwaite, Theodore D et al. (2013). "An improved framework for confound regres-
309 sion and filtering for control of motion artifact in the preprocessing of resting-state
310 functional connectivity data". In: *Neuroimage* 64, pp. 240–256.
- 311 Schaefer, Alexander et al. (2018). "Local-Global Parcellation of the Human Cerebral Cortex
312 from Intrinsic Functional Connectivity MRI". en. In: *Cereb. Cortex* 28.9, pp. 3095–3114.
- 313 Schlemm, Eckhard et al. (2022). "Equalization of Brain State Occupancy Accompanies
314 Cognitive Impairment in Cerebral Small Vessel Disease". en. In: *Biol. Psychiatry* 92.7,
315 pp. 592–602.
- 316 Schulz, Maximilian et al. (2021). "Functional connectivity changes in cerebral small vessel
317 disease - a systematic review of the resting-state MRI literature". en. In: *BMC Med.* 19.1,
318 p. 103.
- 319 Shen, Jun et al. (2020). "Network Efficiency Mediates the Relationship Between Vascular
320 Burden and Cognitive Impairment: A Diffusion Tensor Imaging Study in UK Biobank".
321 en. In: *Stroke* 51.6, pp. 1682–1689.

- 322 Steegen, Sara et al. (2016). "Increasing Transparency Through a Multiverse Analysis". en.
323 In: *Perspect. Psychol. Sci.* 11.5, pp. 702–712.
- 324 Sundaresan, Vaanathi et al. (2019). "Automated lesion segmentation with BIANCA: Im-
325 pact of population-level features, classification algorithm and locally adaptive thresh-
326 olding". en. In: *Neuroimage* 202, p. 116056.
- 327 Tombaugh, Tom N (2004). "Trail Making Test A and B: normative data stratified by age
328 and education". en. In: *Arch. Clin. Neuropsychol.* 19.2, pp. 203–214.
- 329 Tuladhar, Anil M, Ewoud van Dijk, et al. (2016). "Structural network connectivity and cog-
330 nition in cerebral small vessel disease". en. In: *Hum. Brain Mapp.* 37.1, pp. 300–310.
- 331 Tuladhar, Anil M, Jonathan Tay, et al. (2020). "Structural network changes in cerebral small
332 vessel disease". en. In: *J. Neurol. Neurosurg. Psychiatry* 91.2, pp. 196–203.
- 333 Tzourio-Mazoyer, Nathalie et al. (2002). "Automated anatomical labeling of activations in
334 SPM using a macroscopic anatomical parcellation of the MNI MRI single-subject brain".
335 In: *Neuroimage* 15.1, pp. 273–289.
- 336 Vidaurre, Diego et al. (2018). "Discovering dynamic brain networks from big data in rest
337 and task". en. In: *Neuroimage* 180.Pt B, pp. 646–656.
- 338 Wardlaw, Joanna M, Colin Smith, and Martin Dichgans (2013). "Mechanisms of sporadic
339 cerebral small vessel disease: insights from neuroimaging". en. In: *Lancet Neurol.* 12.5,
340 pp. 483–497.
- 341 Wardlaw, Joanna M, Eric E Smith, et al. (2013). "Neuroimaging standards for research
342 into small vessel disease and its contribution to ageing and neurodegeneration". en.
343 In: *Lancet Neurol.* 12.8, pp. 822–838.
- 344 Wardlaw, Joanna M, María C Valdés Hernández, and Susana Muñoz-Maniega (2015). "What
345 are white matter hyperintensities made of? Relevance to vascular cognitive impair-
346 ment". en. In: *J. Am. Heart Assoc.* 4.6, p. 001140.
- 347 Xu, Yuanhang et al. (2021). "Altered Dynamic Functional Connectivity in Subcortical Is-
348 chemic Vascular Disease With Cognitive Impairment". en. In: *Front. Aging Neurosci.* 13,
349 p. 758137.
- 350 Yeo, B T Thomas et al. (2011). "The organization of the human cerebral cortex estimated
351 by intrinsic functional connectivity". en. In: *J. Neurophysiol.* 106.3, pp. 1125–1165.
- 352 Yin, Wenwen et al. (2022). "The Clustering Analysis of Time Properties in Patients With
353 Cerebral Small Vessel Disease: A Dynamic Connectivity Study". en. In: *Front. Neurol.*
354 13, p. 913241.